Supplementary Materials and Methods

Identification of chromatin loops. The cooltools call-dots function, a re-implementation of HICCUPS, was used to *de novo* identify the chromatin loops as described in[1]. Briefly, Hi-C results from six replicates without or with TEV protease treatment in NB buffer, were pooled together and mapped onto hg19 using Distiller pipeline. Then the loops were called at 25kb with the following parameters, fdr = 0.1, clustering-radius 25000, and max-loci-separation 10000000.

Comparison of chromatin loops in different datasets. To compare the loops in our study to those in the published study (8334 loops), we first extended both ends of each loop anchor coordinate from the published dataset by 10kb[2], then we used pairToPair[3] to compare these extended anchors of each loop with the loop coordinates in our dataset. Only both loop anchors from our study overlapping with both loop anchors from the previous dataset were counted as overlapped loops. If neither or only one of two loop anchors of a loop overlaps with the anchors of the loops in the other study, this loop is not counted as an overlapped loop.

Co-Immunoprecipitation (co-IP). Co-IP protocol was adapted from our recent work[4]. Around 40millions of nuclei were incubated in 15ml of NB, NBS0.5, NBS1 or NBS2 buffer, with or without TEV protease treatment at 4°C overnight. To make the description simpler, we used the $RAD21^{TEV}$ nuclei in NBS1 buffer without TEV protease treatment as an example. Briefly, after centrifuged at 1000g in 4°C for 10 minutes, NBS1 buffer was removed and nuclei were resuspended in 900ul of lysis buffer. The lysis and CoIP buffers were prepared based on the corresponding salt buffer with detergent and other chemicals as indicated. For example, for this sample the lysis buffer contains NBS1 with 0.5% NP-40 + protease inhibitor since the nuclei were incubated in NBS1 buffer. The nuclei in lysis buffer was then sonicated using BioRaptor Pico (30sec ON, 30sec OFF, 1 cycle). The sonicated lysate was incubated at 4°C on a rotator for 3 hours after 18ul of Turbonuclease (250U/ul) was added. The lysate was then centrifuged at 10,000g at 4°C for 10mins. Proteins in the supernatant were quantified with BCA and around 1mg of protein was used for the Co-IP. EDTA and DTT were then added to have final concentrations of 1mM for each. 80ul of protein G dynabeads magnetic beads (Thermo Fisher 10004D) were washed once using CoIP buffer (NBS1 + 0.5% NP-40 + 1mM EDTA + 1mM DTT + protease inhibitor), then

added to the 1ml lysate to preclean for 2 hours at 4°C. After this, 1% of input was taken for Western blot analysis. The rest of 1ml lysate was split into two tubes of 500ul for each and 500ul CoIP buffer was added to each tube to make 1ml per tube. Then the lysates were incubated overnight either with 5ug of rabbit IgG (Normal Rabbit IgG, #2729, 1mg/ml) or 5ug CTCF antibodies (Millipore, #07-729, 1mg/ml). The next day, 40ul of protein G dynabeads were first washed once in CoIP buffer and then added to each tube and incubated 2 hours at 4°C on a rotator. The beads were then washed 5 times with 1ml Co-IP buffers for 3mins using a magnetic rack at room temperature. To elute the proteins, the beads were resuspended in 35ul of 2x sample buffers (diluted from 5x sample buffer, Thermo Fisher, #39000), heated for 5min at 100°C and the supernatants were taken after placing the tubes on the magnetic rack. 8-10ul of the samples was used to analyze a target protein using Western blot.

SILAC labeling and analysis

Details for our SILAC analysis can be found in our previous work[5]. Briefly, on day 0, early-passage HAP1-RAD21^{TEV} cells were grown in IMDM for SILAC (Thermo Fisher, #88367), which contained L-Arginine-$^{13}C_6$ hydrochloride (Sigma 643440-100MG) and L-LYSINE:2HCL (4,4,5,5-D4, 96-98%, Cambridge Isotope DLM-2640-0.1). Unlabeled HAP1-RAD21^{TEV} cells were grown in light IMDM SILAC media, which contained L-arginine (Arg0) and L-lysine (Lys0) (Sigma). Cells were grown for more than 10 d (>3 passages) to allow for sufficient incorporation of the isotopes. On day 11, cells were lysed using RIPA buffer with Turbonuclease (250U/ul) and protease inhibitor. After centrifuged at 10,000g at 4°C for 10mins, the protein concentrations were determined using BCA assay (Thermo, #23225). 2x Laemmli buffer (BioRad, #1610737) with 0.1M DTT was then added into the lysates and the lysate with 25-50ug proteins were loaded onto a 4-10% SDS PAGEs after heated at 100°C for 5mins. After all the lysates entered the gel, the Coomassie-stained protein bands were excised and collected for incorporation analysis. The results indicated more than 98% of peptides were incorporated with Arginine/Lysine containing C13.

Around 15 millions of nuclei were prepared from either labeled or label-free HAP1-RAD21^{TEV} cells and plated on 10cm poly-D-lysine coated plates (Corning, #356469) with HBSS buffer at 4°C overnight. The labeled nuclei were treated with 15U/ml TEV protease for overnight. The next day, both labeled and label-free nuclei were incubated with 200ul RIPA lysis buffer with Turbonuclease and protease inhibitor at 4°C for 10mins, then the lysates were collected and the

protein concentrations were determined by BCA. 2x Laminlia buffer with 0.1M DTT was added and boiled at a 100°C heat block. The labeled and label-free lysates were then mixed in a 1:1 ration (M:L) and loaded on a 4-12% SDS-PAGE. A fully resolved SDS–PAGE gel was cut into five fractions, and each fraction was processed and analyzed for LC-MS/MS separately. More detailed information for MS sample preparation and LC-MS/MS analysis can be found in our previous study[5]. After the raw MS data was processed with Mascot Distiller, SILAC ratio quantitation was loaded into the Scaffold Viewer for peptide/protein validation. For SILAC experiments, protein identification was subject to a two-peptide cutoff. For proteins detectable in the labeled sample (M) but lacking an empirical M/L ratio value (owing to low background detection in the label free sample (L)), peak areas of all the identified peptides in the Distiller file were used to calculate H/L ratios. The fold change and BH-adjusted P values for CTCF and each cohesin subunit were extracted to compare to fold changes obtained from Western blot using nuclei in NBS1 buffer.

Supplementary Figure Legends

Supplementary Fig 1. A replicate Hi-C analysis of the nuclei with cleaved RAD21 in NBS1

(a) Hi-C interaction maps for HAP1-RAD21^{TEV} nuclei without and with TEV protease treatment in NB or NBS1, respectively. Data for the 18-107.3 Mb region of chromosome 14 is shown at 200kb resolution. Right panels, 132mM NaCl was added to NB buffer during TEV protease treatments at 4°C overnight. Bottom, eigenvector E1 across the 18-107.3 Mb region of chromosome 14 at 200kb resolution. **(b)** Saddle plots of Hi-C data binned at 200kb for HAP1-RAD21^{TEV} nuclei without and with TEV treatment in NB or NBS1, respectively. The numbers indicate compartment strength. **(c)** Interaction strength of compartments. The bars represent the strength of compartment interactions for each sample as indicated. Dark bars, strength of AA interaction as compared to AB interaction (A-A/A-B). Grey bars, strength of BB interaction as compared to AB interaction (B-B/B-A). **(d)** Hi-C interaction maps for salt effects on HAP1-RAD21^{TEV} nuclei without and with TEV protease treatment in NB or NBS1, respectively. Data for the 29-34 Mb regioncof chromosome 14 is shown at 20kb resolution. Middle panels, insulation profiles for the 29-34 Mb regions of chromosome 14 at 20kb resolution. The lower panels indicate compartment Eigenvector value E1 across the same region at 200kb resolution. **(e)** Aggregate Hi-C data binned at 20kb resolution at TAD boundaries identified in the sample in NB buffer without

TEV treatment in NB or NBS1. The numbers at the sides of the cross indicate the strength of boundary-anchored stripes using the mean values of interaction frequency within the white dashed boxes, as in Extended Data Fig. 1h. **(f)** *P(s)* plots (left panels), and the derivatives of *P(s)* plots (right panels) for Hi-C data from nuclei with or without TEV treatment as indicated. The blue arrows indicate the signature of cohesin loops in each condition. The red arrows indicate the changes of contact frequency at 2Mb. (**g**) Aggregated Hi-C data binned at 20kb resolution at loops as in Fig. 2j. Lower panels: average Hi-C signals along the blue dashed line shown in the upper left Hi-C panel. **(h)** Aggregated Hi-C data binned at 20kb resolution at chromatin loops of three different loop sizes, 100-500kb, 500kb-1Mb, and >1Mb. Lower panels: average Hi-C signals along the blue dashed line shown in the left Hi-C map in panel Fig. 2j.

Supplementary Fig. 2 is an independent replicate of Extended Data Fig 7. See Extended Data Fig. 7 for legend.

Supplementary Fig. 2 is an independent replicate of Extended Data Fig 8. See Extended Data Fig. 8 for legend.

Supplementary Fig. 4. A biological replicate for compartmentalization analysis after nuclear expansion and contraction

(a) Changes of nuclear morphology during the expansion and contraction assay. Upper panel: a schematic to show nuclear morphology changes before expansion, after expansion, and after expansion followed by compaction. Middle and bottom, images of HAP1-RAD21^{TEV} nuclei before expansion, after expansion, and after expansion followed by compaction without and with TEV protease treatment, respectively (Scalebar =100μm). **(b)** Hi-C interaction maps for HAP1-RAD21^{TEV} nuclei before expansion, after expansion, and after expansion followed by compaction without and with TEV protease treatment, respectively. Data for the 18-107.3 Mb region of chromosome 14 is shown at 200kb resolution. Lower panels: Eigenvector E1 across the 18-107.3 Mb region of chromosome 14 at 200kb resolution. The blue, red and grey lines represent before expansion, after expansion, and after expansion followed by compaction treatments, respectively. Blue arrows indicate E1 changes. Bottom panels, E1 across the 77.8-98Mb region of chromosome 14 at 200kb resolution. **(c)** Saddle plots of Hi-C data binned at 200kb for RAD21^{TEV} nuclei before

expansion, after expansion, and after expansion followed by compaction without and with TEV protease treatment, respectively. The numbers indicate compartment strength. **(d)** Interaction strength of compartments. The bars represent the strength of compartment interactions for each sample as indicated. Dark bars, strength of AA interaction as compared to AB interaction (A-A/A-B). Grey bars, strength of BB interaction as compared to AB interaction (B-B/B-A).

Supplementary Fig. 5. A biological replicate for Hi-C analysis after nucleus expansion and contraction

(a) Hi-C interaction maps for HAP1-RAD21^{TEV} nuclei before expansion, after expansion, and after expansion followed by compaction without and with TEV protease treatment, respectively. Data for the 29-34 Mb region of chromosome 14 is shown at 20kb resolution. **(b)** Insulation profiles for the 29-34 Mb regions of chromosome 14 at 20kb resolution. The blue, red and grey lines represent before expansion, after expansion, and after expansion followed by compaction treatments, respectively. The blue arrows indicate weakened insulation boundary as nuclei was expanded. The lower panels indicate compartment Eigenvector value E1 across the same region at 200kb resolution. **(c)** Aggregate Hi-C data binned at 20kb resolution at TAD boundaries identified in control sample without TEV treatment. The numbers at the sides of the cross indicate the strength of boundary-anchored stripes using the mean values of interaction frequency within the white dashed boxes, as in Extended Data Fig. 1h. (**d**) Aggregated Hi-C data binned at 20kb resolution at loops as used in Fig. 2j. Right panels: average Hi-C signals along the blue dashed line shown in the left upper Hi-C panel. **(e)** *P(s)* plots (upper panels), and the derivatives of *P(s)* plots (lower panels) for Hi-C data from nuclei before expansion, after expansion, and after expansion followed by compaction without and with TEV protease treatment, as indicated. The blue arrows indicate the signature of cohesin loops in each condition. The red arrows indicate the changes of contact frequency at 2Mb.

Supplementary Fig. 6. (a) Western blot analysis of nuclear retention of cohesin subunits and CTCF in RAD21^{WT} nuclei in NB, NBS1 or NBS2 buffer (see Methods for nuclear retention assay for detail). LMNA was used as loading controls to normalize each cohesin component and CTCF in the same lane. The left panel shows levels of each cohesin subunit and CTCF in each condition that were then normalized to its level in nuclei in NB to calculate fold changes. Relative levels of

subunits retained in nuclei are shown under each LMNA blot for each subunit or CTCF. The right panel indicates levels of each cohesin subunit and CTCF that were released into supernatant in different salt buffers as indicated. **(b)** The strength of CTCF-CTCF loop and intra-TAD interactions in $RAD21^{WT}$ nuclei. The heat maps in the first and second rows indicate the aggregate Hi-C data binned at 20kb resolution at the loops identified in HAP1 cells (8,334, Sanborn et. al, PNAS, 2015). The plot in the second row shows the loop line that indicates the average Hi-C signals along the dotted blue lines representing signals from the bottom-left corner to the top-right corner of the loop aggregated heat maps shown in the first and second rows. The blue, red and gray lines represent the signals in NB, NBS1 and NBS2 buffers, respectively. The lower panel shows quantification of loop strength and intra-TAD interaction strength. (See Fig 1bc for measurement of loop and intra-TAD interaction strength). **(c)** The cell cycle profiles of $RAD21^{WT}$ and $RAD21^{TEV}$ cells. The upper panels show the cell cycle profiles of HAP1-$RAD21^{WT}$ cells in early (left panel) and late (right panel) passages. The lower panels indicate the cell cycle profiles of HAP1-$RAD21^{TEV}$ cells in early and late passages, left and right panels, respectively. The percentage for each cell cycle phase are indicated. The PI staining intensities are used to indicate the DNA contents. **(d)** Profiles of ChIP signals of CTCF at the combined CTCF binding sites that were identified from the $RAD21^{WT}$ and $RAD21^{TEV}$ nuclei plated in NB buffer overnight. In total, 27,406 CTCF binding sites were identified in either $RAD21^{WT}$ or $RAD21^{TEV}$ nuclei, among which, 20,616 CTCF binding sites were detected as CTCF binding sites in both $RAD21^{WT}$ and $RAD21^{TEV}$ nuclei (cyan line), while 1,527 (dark blue line) and 5,263 (yellow line) CTCF binding sites were detected only in $RAD21^{WT}$ or only $RAD21^{TEV}$ nuclei, respectively. The first column is a profile of CTCF ChIP signals at the combined 27,406 CTCF sites in $RAD21^{WT}$ nuclei in NB buffer. The rest four columns indicate the profiles of CTCF ChIP signals at the combined 27,406 CTCF binding sites in $RAD21^{TEV}$ nuclei with and without TEV protease treatment in NB or NBS1 buffer. Upper panel, the average CTCF ChIP signals of each condition for these 27,406 CTCF binding sites. Lower panel, stack-up heatmap of CTCF ChIP signals for each condition at each of 27, 406 CTCF binding sites. **(e)** Profiles of ChIP signals of RAD21 at the combined RAD21 binding sites that were identified from the $RAD21^{WT}$ and $RAD21^{TEV}$ nuclei plated in NB buffer overnight. In total, 18,190 RAD21 binding sites were identified in either $RAD21^{WT}$ or $RAD21^{TEV}$ nuclei, among which, 12,078 RAD21 binding sites were detected as RAD21 binding sites in both $RAD21^{WT}$ and $RAD21^{TEV}$ nuclei (cyan line), while 4,064 (dark blue line) and 2,048 (yellow line) RAD21 binding

sites were detected only in RAD21^{WT} or only RAD21^{TEV} nuclei, respectively. The first column is a profile of RAD21 ChIP signals at the combined 18,190 RAD21 sites in the RAD21^{WT} nuclei in NB buffer. The rest four columns indicate the profiles of RAD21 ChIP signals at the combined 18,190 RAD21 sites in the RAD21^{TEV} nuclei with and without TEV protease treatment in NB or NBS1 buffer. Upper panel, the average RAD21 ChIP signals of each condition for these 18,190 CTCF binding sites. Lower panel, stack-up heatmap of RAD21 ChIP signals for each condition at each of 18,190 RAD21 binding sites. **(f)** Aggregate Hi-C data binned at 20kb resolution at loops identified in HAP1 nuclei and cells. The heat maps show the Hi-C data from HAP1-RAD21^{TEV} nuclei after overnight plating (ON), freshly prepared HAP1-RAD21^{TEV} nuclei (FN) and HAP1-RAD21^{WT} cells. Lower plot: the loop line profile for ON, FN and RAD21^{WT} cells, respectively. **(g)** *P(s)* plots (upper panels), and the derivative of *P(s)* plots (lower panel) for Hi-C data from ON, FN and RAD21^{WT} cells as indicated. The blue, red and gray lines represent ON, FN and RAD21^{WT} cells, respectively. **(h)** Eigenvector value E1 across chromosome 14 at 200kb resolution. From upper to lower panels, E1 profiles of chromosome 14 from ON, FN and RAD21^{WT} cells. **(i)** Comparison of E1 values from FN or RAD21^{WT} cells to those from ON. Left panel, FN vs. ON, right panel, RAD21^{WT} vs. ON. The correlation coefficient (R) is shown on the top right corner on each panel. **(j)** The bar plot shows the numbers of loops that were identified from RAD21^{TEV} nuclei in NB buffer without or with TEV protease treatment. From the pooled Hi-C data of six independent biological replicates, 2,819 loops were identified without TEV protease treatment. After TEV treatment, 819 loops were detected. **(k)** Comparison of the loops identified from our study to those in the previous study (Sanborn, PNAS 2015). The Venn diagram shows that 2024 loops overlap with 1964 loops identified from the previous study. 795 and 6370 loops were identified from our study (NB) and previous study (HAP1-WT), respectively. The 8334 loops in the previous study were used for aggregate loop analysis in our study[2].

Supplementary Fig. 7. Comparison of the aggregate Hi-C data binned at 20kb resolution at the different loops shown in Supplementary Fig. 6k. NB-only, Shared and Cells-only indicate loops identified only from our study (left column), both studies (middle column) and the previous study[2] (right column), respectively. The results include Hi-C data from NB, NBS1 and NBS2 buffers without or with TEV protease treatment as indicated. The plots indicate the loop line profiles for each condition (See Fig. 1b for loop line calculation). Blue and red lines represent without and

with TEV protease treatment, respectively. **(a)** and **(b)** indicate two independent biological replicates.

Supplementary Fig. 8. (a) The morphology of nuclei after expansion for different time or after expansion and contraction, without and with TEV protease treatment. The first and second rows show without and with TEV protease treatment respectively. From left to right, they are control nuclei (I and VIII) without expansion, the nuclei after expansion for 1, 2, 4, 6, and 8 hours as indicated (II-VI and IX- XIII), and the nuclei after 4 hour expansion and 1 hour contraction (VII and XIV) (Scalebar =100μm). **(b)** The relative area of the nuclei after expansion and contraction in each condition for one representative biological replicate (n=1) as indicated. The nuclei after 4 hour expansion are indicated by red arrows. **(c)** Western blot analysis of chromatin affinities of cohesin subunits and CTCF in the nuclear expansion and contraction assays. The antibodies that recognized the N-terminal of RAD21, CTCF, SMC1 and SMC3 were used to detect the protein levels after the nuclei were expanded for 1, 2 and 4 hours as indicated. The nuclei that were not expanded and the nuclei that were contracted for 1 hour after 4 hour expansion are shown as controls. For each blot, lane 1-5 and lane 6-10 indicate without and with TEV protease treatment, respectively. **(d)** Effects of salt concentrations on the cleaving efficiency of TEV proteases. The nuclei in different salt buffers were treated with TEV proteases for 1, 2, 4 (hours), and overnight, then the nuclei in each condition were lysed and analyzed by Western blot. Levels of un-cleaved bands of $RAD21^{TEV}$ indicate the efficiency of TEV cleaving. The experiment was performed in three different salt buffers, NB, NBS1 (NB + 132mM NaCl), and NBS2 (NB+200mM NaCl). **(e)** Quantitation of relative levels of un-cleaved $RAD21^{TEV}$ shown in **(d)**. Levels of LMNA were used to normalize the levels of un-cleaved $RAD21^{TEV}$ in the same lane. Normalized levels of un-cleaved $RAD21^{TEV}$ in each condition in the same buffer were then further normalized to the levels of un-cleaved $RAD21^{TEV}$ without TEV protease treatment for 2 hours in each buffer (First lane in each blot). The blue, red and gray lines represent NB, NBS1 and NBS2, respectively. **(f)** Profiles of ChIP signals of CTCF and RAD21 at the combined CTCF binding sites that were identified from the freshly prepared (FN) and overnight-plated (ON) $RAD21^{TEV}$ nuclei in NB buffer. In total, 29,874 CTCF binding sites were identified in either FN or ON, among which, 22,351 CTCF binding sites were detected as CTCF binding sites in both FN and ON (cyan line), while 2995 (dark blue line) and 3528 (yellow line) CTCF binding sites were detected only in FN or ON,

respectively. The first column is a profile of CTCF ChIP signals at the combined 29,874 CTCF sites in FN in NB buffer. The rest four columns indicate the profiles of CTCF ChIP signals at the combined 29,874 CTCF binding sites in the ON without and with TEV protease treatment in NB or NBS1 buffer. Upper panel, the average CTCF ChIP signals of each condition for these 29,874 CTCF binding sites. Lower panel, stack-up heatmap of CTCF ChIP signals for each condition at each of 27, 406 CTCF binding sites. Right panel, profile of RAD21 ChIP signals at the combined 29,874 CTCF binding sites in the ON without and with TEV protease treatment in NB or NBS1 buffer. Upper panel, the average RAD21 ChIP signals of each condition for these 29,874 CTCF binding sites. Lower panel, stack-up heatmap of RAD21 ChIP signals for each condition at each of 29,874 CTCF binding sites. **(g)** and **(h)** Western blot analysis for CoIP against CTCF in $RAD21^{TEV}$ nuclei without or with TEV protease treatment in different buffers. CoIP was performed against CTCF in $RAD21^{TEV}$ nuclei in NB, NBS0.5, NBS1 and NBS2 buffers, which contain 0, 66, 132 and 200mM NaCl, respectively. I, IgG and IP indicate input, CoIP using control IgG antibodies, CoIP using CTCF antibodies, respectively. Antibodies against CTCF and cohesin subunits as indicated were used to detect levels CTCF and cohesin subunits after CoIP. Two independent biological replicates were performed and here it shows a representative replicate.

Supplementary Fig. 9. Analysis of nucleus morphology in different buffer conditions. **(a)** Nuclear morphology in hypotonic buffers (10mM HEPES, pH 7.4) with different concentrations of $MgCl_2$. Left panel, the first and second rows of images indicate $RAD21^{TEV}$ nuclei without and with TEV protease treatment. Nuclei in HBSS (I and II) and HEPEs (III and IV) buffers are negative and positive controls, respectively. The rest indicate the nuclear morphology in HEPES buffer with different concentrations of $MgCl_2$ as indicated. Right panel, a box plot shows nuclear cross-sectional area changes in different buffers. The area of 30 nuclei from the left panels in each condition was measured and plotted using image J and R. Median cross-sectional area in HBSS buffer without TEV protease treatment was set at 1, and fold change in area is shown for nuclei in each condition. All the nuclei were first plated in HBSS buffer at 4°C overnight, then were washed twice and incubated in the indicated buffers for 4 hours at room temperature before images were taken. (Scalebar =100μm) **(b)**. Nuclear morphology in hypotonic buffers (10mM HEPES, pH 7.4) with different concentrations of KCl and 2mM $CaCl_2$. Left panel, the first and second rows of images indicate $RAD21^{TEV}$ nuclei without and with TEV protease treatment. Nuclei in HBSS (I

and II) and HEPEs (III and IV) buffers are negative and positive controls, respectively. The rest images indicate the nuclear morphology in HEPES buffer with different concentrations of KCl and 2mM $CaCl_2$ as indicated. Right panel, a box plot shows nuclear cross-sectional area changes in different buffers. The area of 30 nuclei from the left panels in each condition was measured and plotted using image J and R. Median cross-sectional area in HBSS buffer without TEV protease treatment was set at 1, and fold change in area is shown for nuclei in each condition. All the nuclei were first plated in HBSS buffer at 4°C overnight, then were washed twice and incubated in the indicated buffers for 4 hours at room temperature before images were taken. (Scalebar =100μm) **(c)** Nuclear morphology in expansion and contraction assays. Left panel, the first row of images indicates the morphology $RAD21^{TEV}$ nuclei after the expansion and contraction assay as described in methods. Briefly, all the nuclei in **(c)** were plated in HBSS at 4°C overnight, and then washed twice with HBSS (I) or expansion buffer (10mM HEPEs pH 7.4 and 1mM EDTA, II-XI) before they were incubated in HBSS or expansion buffers for 4 hours as indicated. For nuclei in III or IV-XI, after 4 hour expansion, they were incubated in HBSS (III) or HEPES (10mM, pH 7.4) buffers with different concentrations of KCl or NaCl (IV-XI) as indicated for 1 hour. Right panel, a box plot shows nuclear cross-sectional area changes in different buffers. The area of 30 nuclei from the left panels in each condition was measured and plotted using image J and R. Median cross-sectional area in HBSS buffer without expansion was set at 1, and fold change in area is shown for nuclei in each condition. (Scalebar =100μm) **(d)** Nuclear morphology in different buffers. Left panel, the first and the second rows of images indicate the morphology $RAD21^{TEV}$ nuclei without and with TEV protease treatment in different buffers as indicated. The nuclei were plated in the indicated buffers at 4°C overnight before images were taken. Right panel, a box plot shows nuclear cross-sectional area changes in different buffers. The area of 30 nuclei in each condition was measured and plotted using image J and R. Median cross-sectional area from the left panels in NB buffer without TEV protease treatment was set at 1, and fold change in area is shown for nuclei in each condition. (Scalebar =100μm) **(e)** Nuclear morphology in an expansion and contraction assay. Left panel, the first and the second rows of images indicate the morphology $RAD21^{TEV}$ nuclei without and with TEV protease treatment in different buffers as indicated. All the nuclei here were plated in HBSS at 4°C overnight, and then washed twice with HBSS (I & IV) or expansion buffer (10mM HEPES pH 7.4 and 1mM EDTA, II-VI) at room temperature for 4 hours. After expansion, the nuclei in III and VI were incubated in HBSS buffer containing 3.2mM EDTA at room

temperature for 1 hour. Right panel, a box plot shows nuclear cross-sectional area changes in different buffers. The area of 30 nuclei from the left panels in each condition was measured and plotted using image J and R. Median cross-sectional area in HBSS buffer without TEV protease treatment was set at 1, and fold change in area is shown for nuclei in each condition. (Scalebar =100μm). All nucleus morphology images and corresponding box plots represent one of two independent biological replicates.

Supplementary Fig. 10. Western blot analysis of nuclear retention of CTCF and cohesin in RAD21TEV nuclei without and with TEV protease treatment in low salt (NB), physiological salt (NBS1), or high salt (NBS2) buffers. The left and right columns indicated two replicates. For each protein as indicated, the upper and lower blots represent the protein and the loading control (LAMIN A). For each blot, including the loading control blot, the first three bands are calibration bands, with increased loading volume as shown above the blot. The subsequent six bands are the proteins without and with TEV protease treatment in different buffers, from left to right, NB, NBS1 and NBS2 buffers. All the calibration bands for each protein and loading control are on the same blot with the sample bands, except the calibration bands for the SA2 and its loading control in the replicate 1 (the left bottom). The calibration bands are from another blot as shown in a separate small blot at the left bottom. The numbers of under each loading control blot indicate the fold change of each cohesin subunit and CTCF in each condition as indicated (See method or Fig.3a for calculation of fold change)

Supplementary Fig. 11. (a) The summary box plots for all the replicate experiments of nuclei retention assays. The relative fold changes for protein X were obtained using the following formula:

$$(\text{Protein X levels} / \text{LMNA levels})^{\text{Condition}} / (\text{Protein X levels} / \text{LMNA levels})^{\text{NB without TEV}}$$

Protein X = CTCF or RAD21 or other cohesin component

Condition = NB with TEV; NBS1 without or with TEV; NBS2 without or with TEV.

FC in each panel represent the fold changes of (NBS1 +TEV / NBS1 no TEV) and *p* values were obtained using Student t test (one-sided). The "n" represents the times of independent biological replicates. **(b)** Correlation of SILAC results with average fold changes obtained from Western

blots. The blue dots in the left part of the panel represent fold changes of cohesin subunit and CTCF from two independent SILAC analyses in the HBSS buffer. The red dots in the right part show the fold changes for each protein obtained from Western blots. **(c)** Western blot analysis of RAD21 in the HCT-116 cells without and with CRISPR modifications. From the left to the right, RAD21 from the wild-type HCT116 cells, the HCT116 cells tagged with TIR2 at the AAVS1 site, the HCT116 cells tagged with AID-clover inserted into RAD21, HCT116-AID-mClover cells (having TIR2 at AAVS1 and AID-Clover inserted into RAD21, used in Fig.1), and HCT116-AID-mClover with auxin treated for 2 and 4 hours. The last three bands are calibration bands for HCT116-AID-mClover. The LMNA bands were used as loading controls.

Supplementary Fig. 12. (a) Comparison of CTCF and nRAD21 ChIP peaks. From CTCF and nRAD21 ChIP results, 25,879 and 14,126 peaks were identified using HOMER (See methods), respectively. 13,422 peaks (95%) of 14,126 nRAD21 peaks overlap with CTCF peaks. Among the non-overlapping peaks, 130 peaks have a distance of less than 2kb from the nearest CTCF peaks, while 574 peaks are more than 2kb away from the nearest CTCF peaks. The Venn diagram shows the percentages of the nRAD21 peaks either overlapping or non-overlapping with CTCF peaks. Among these 574 peaks, 411 are more than 2kb away from active TSS sites. The right panel shows the profiles of the CTCF and nRAD21 ChIP signals at these 411 nRAD21 peaks 2kb in each condition as indicated. **(b)** Similar with **(a)**, this panel shows the comparison of CTCF and cRAD21 ChIP peaks. From cRAD21 ChIP results, 14,683 peaks were called using HOMER. 13,887 peaks (95%) of 14,683 cRAD21 peaks overlap with CTCF peaks. Among the non-overlapping peaks, 114 peaks have a distance of less than 2kb from the nearest CTCF peaks, while 682 peaks are more than 2kb away from the nearest CTCF peaks. The Venn diagram shows the percentages of the nRAD21 peaks either overlapping or non-overlapping with CTCF peaks. Among these 682 peaks, 460 are more than 2kb away from active TSS sites. The right panel shows the profiles of the CTCF and nRAD21 ChIP signals at the 460 nRAD21 peaks in each condition as indicated. **(c)** Comparison of loop and intra-TAD interaction strength in $RAD21^{TEV}$ nuclei without and with TEV treatment in the NBS1 buffer. The upper and lower panels show two replicates respectively. In each panel, the left two bars represent the loop interaction strength while the right two bars indicate the intra-TAD interaction strength. The dark and gray color indicate without and with TEV protease treatments respectively.

REFERENCES

1 Akgol Oksuz, B. *et al.* Systematic evaluation of chromosome conformation capture assays. *Nat Methods* **18**, 1046-1055, doi:10.1038/s41592-021-01248-7 (2021).

2 Sanborn, A. L. *et al.* Chromatin extrusion explains key features of loop and domain formation in wild-type and engineered genomes. *Proc Natl Acad Sci U S A* **112**, E6456-6465, doi:10.1073/pnas.1518552112 (2015).

3 Quinlan, A. R. & Hall, I. M. BEDTools: a flexible suite of utilities for comparing genomic features. *Bioinformatics* **26**, 841-842, doi:10.1093/bioinformatics/btq033 (2010).

4 Valton, A.-L. *et al.* A cohesin traffic pattern genetically linked to gene regulation. *bioRxiv*, doi:10.1101/2021.07.29.454218 (2021).

5 Gao, X. D. *et al.* C-BERST: defining subnuclear proteomic landscapes at genomic elements with dCas9-APEX2. *Nat Methods* **15**, 433-436, doi:10.1038/s41592-018-0006-2 (2018).

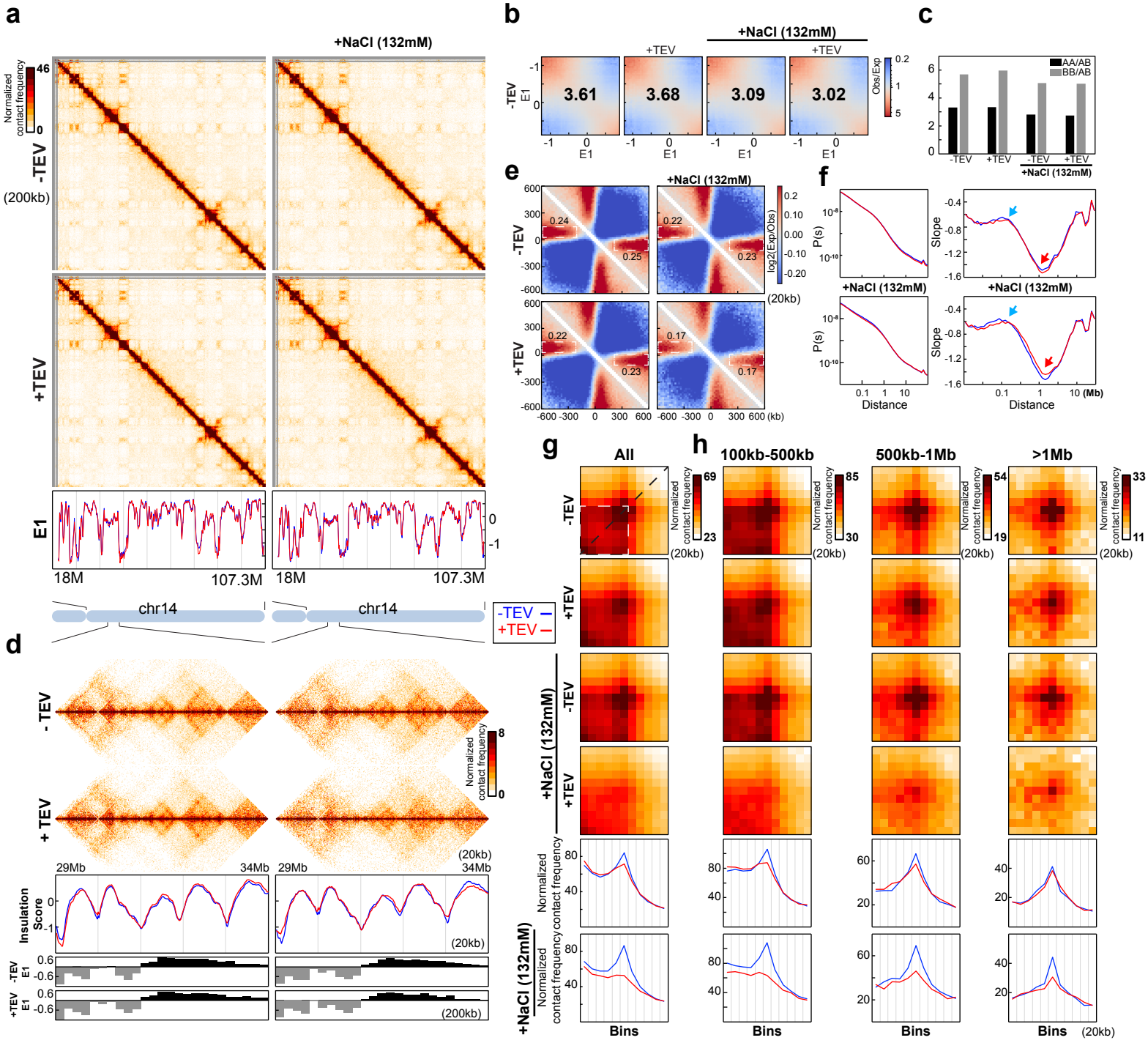

Supplementary Fig. 1

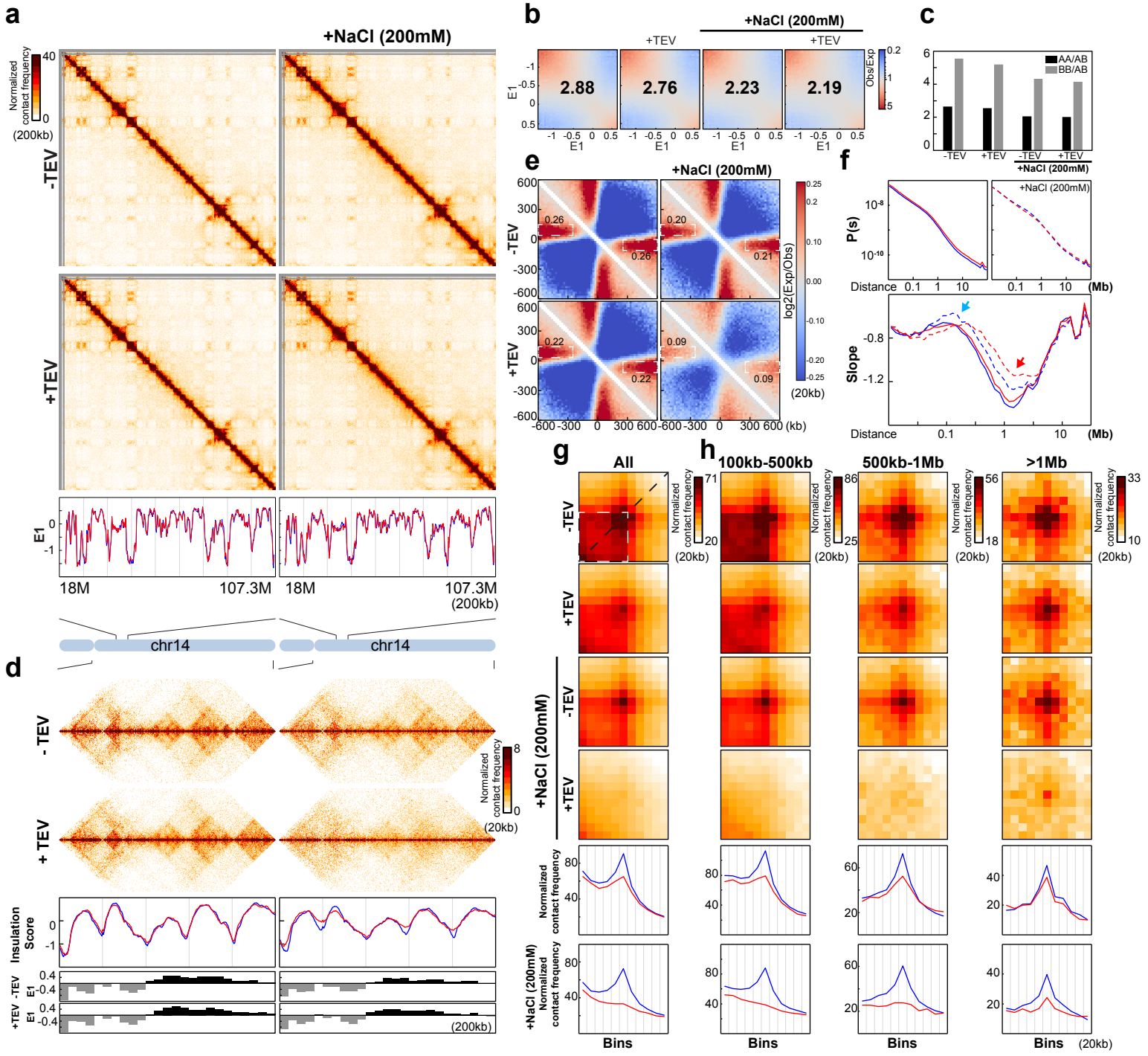

Supplementary Fig. 2

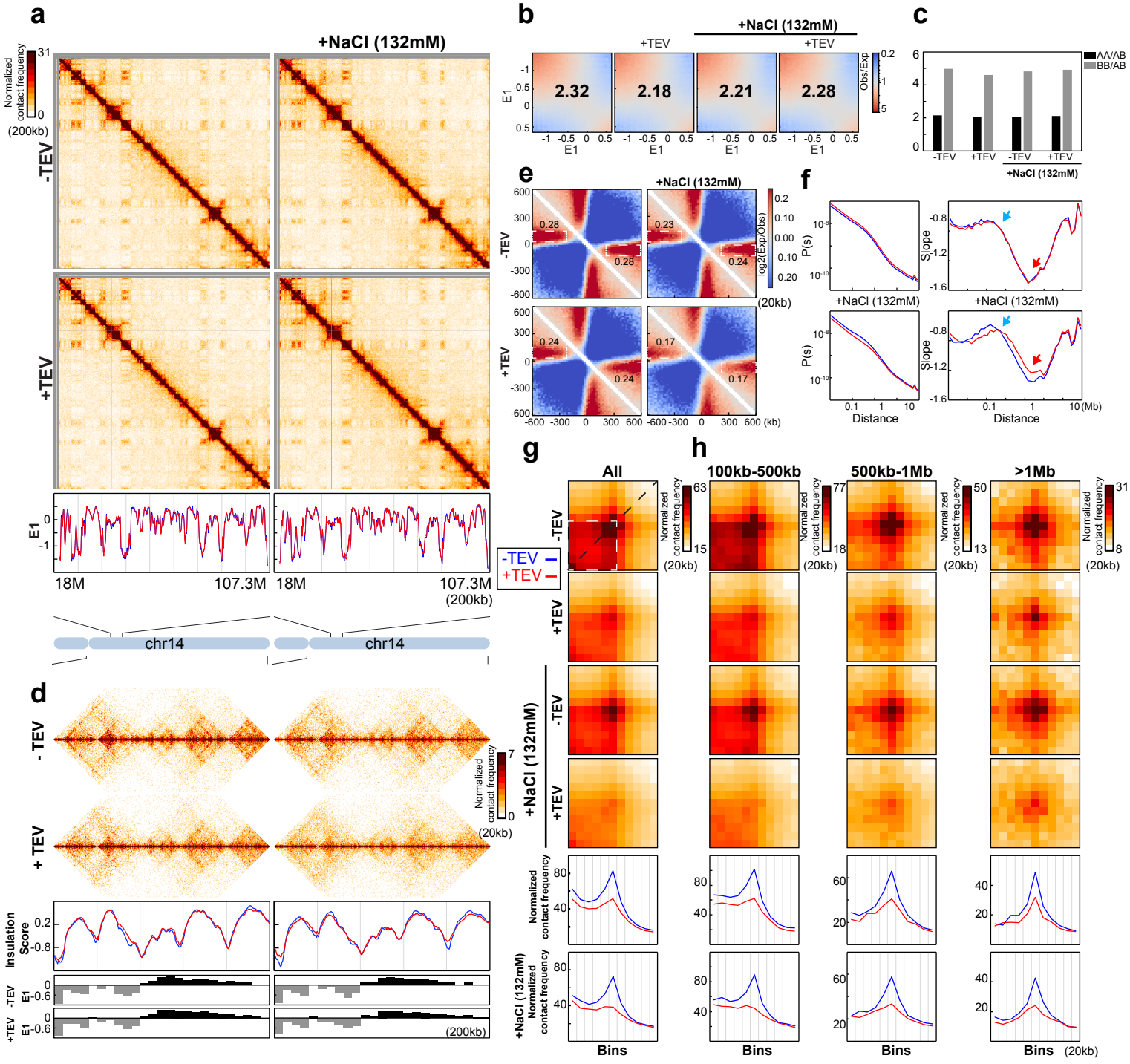

Supplementary Fig. 3

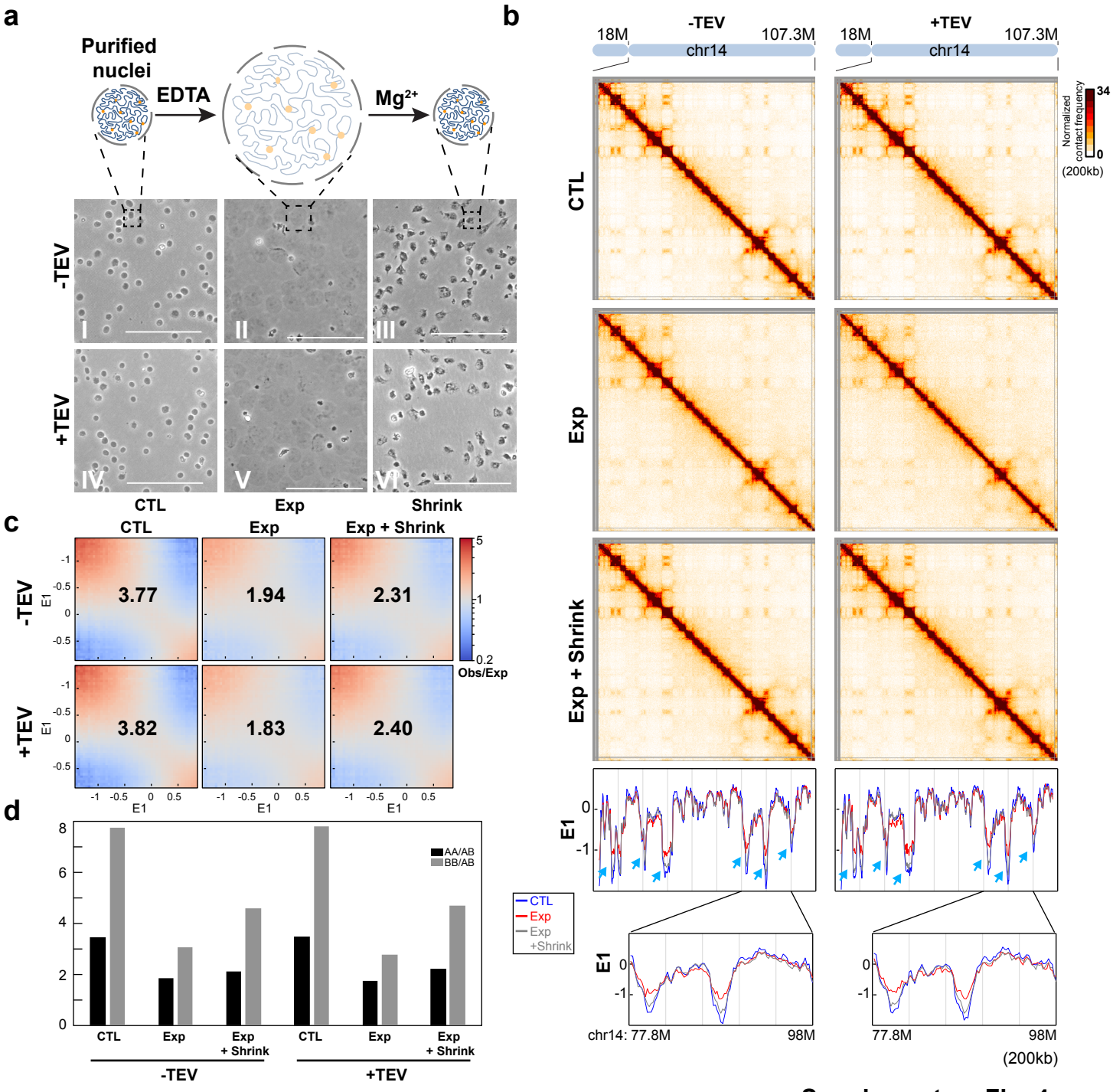

Supplementary Fig. 4

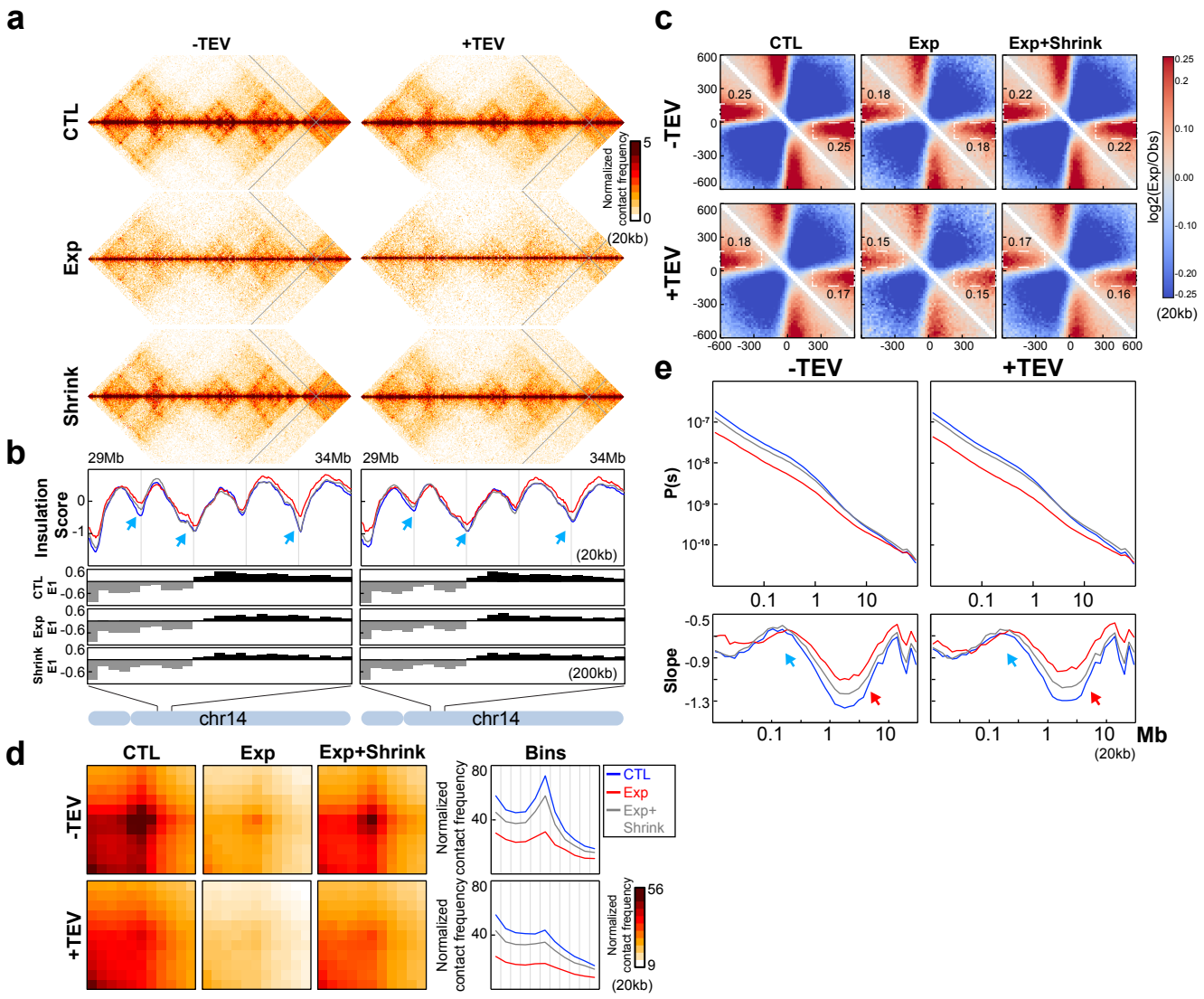

Supplementary Fig. 5

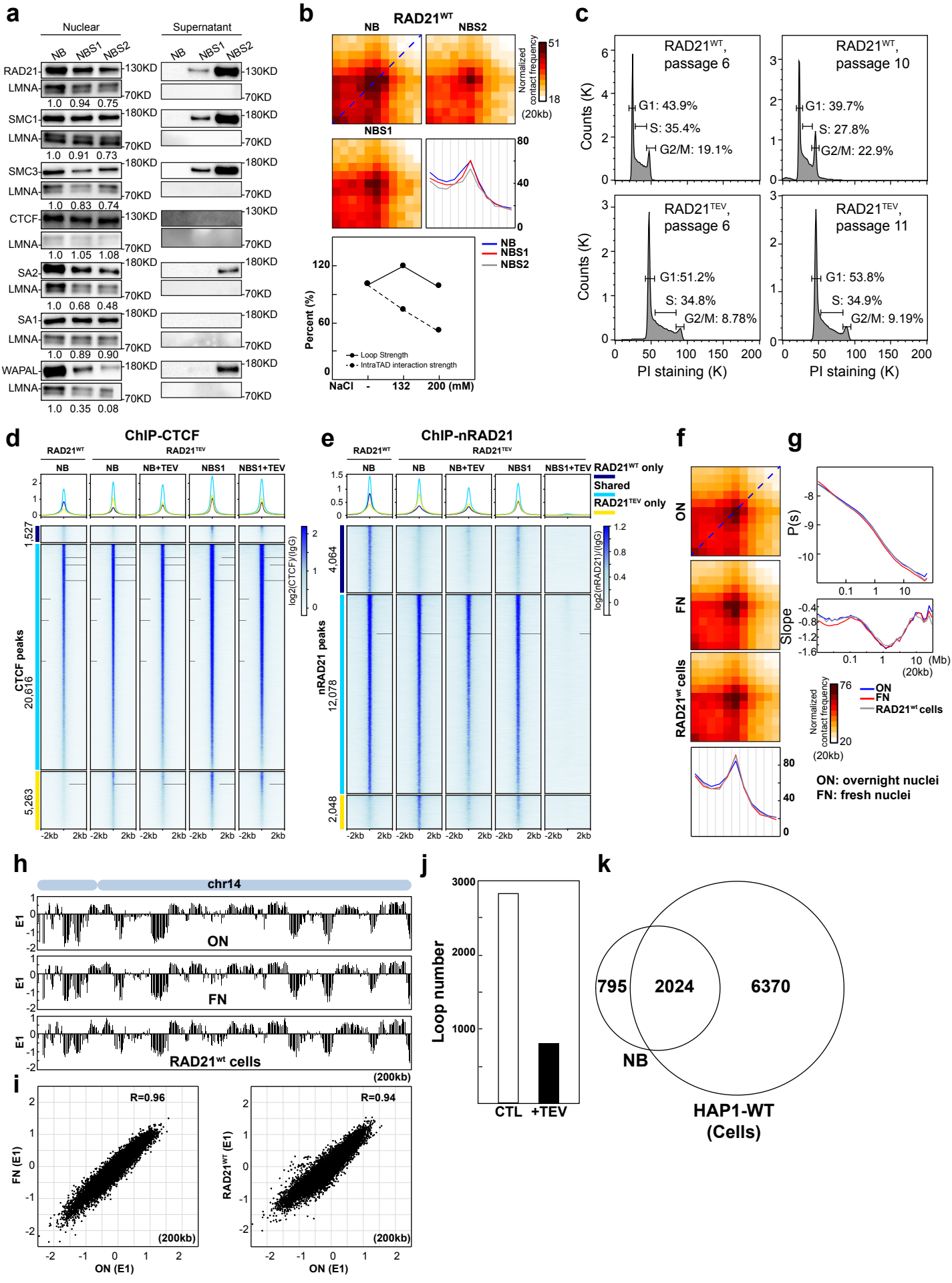

Supplementary Fig. 6

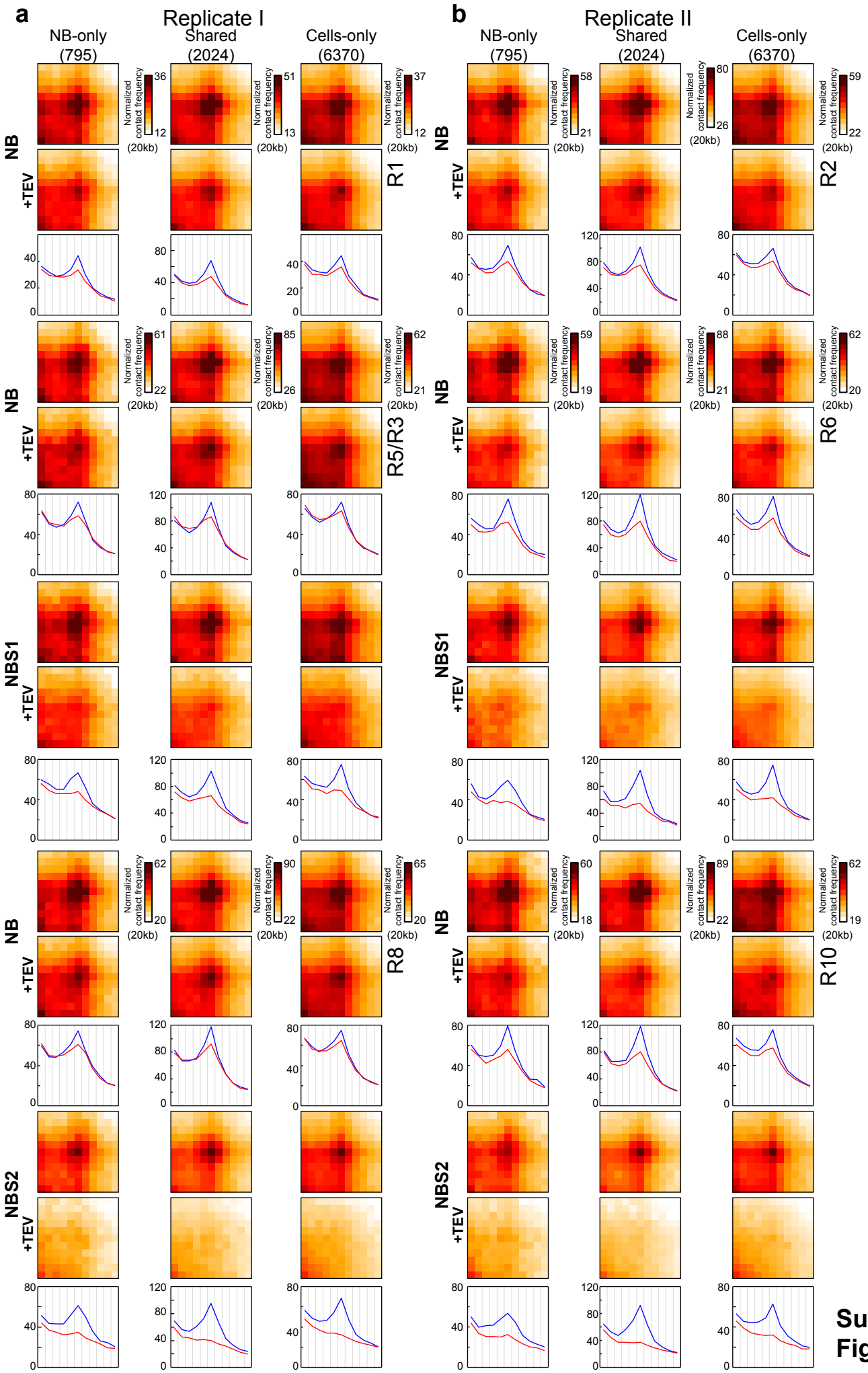

Supplementary Fig. 7

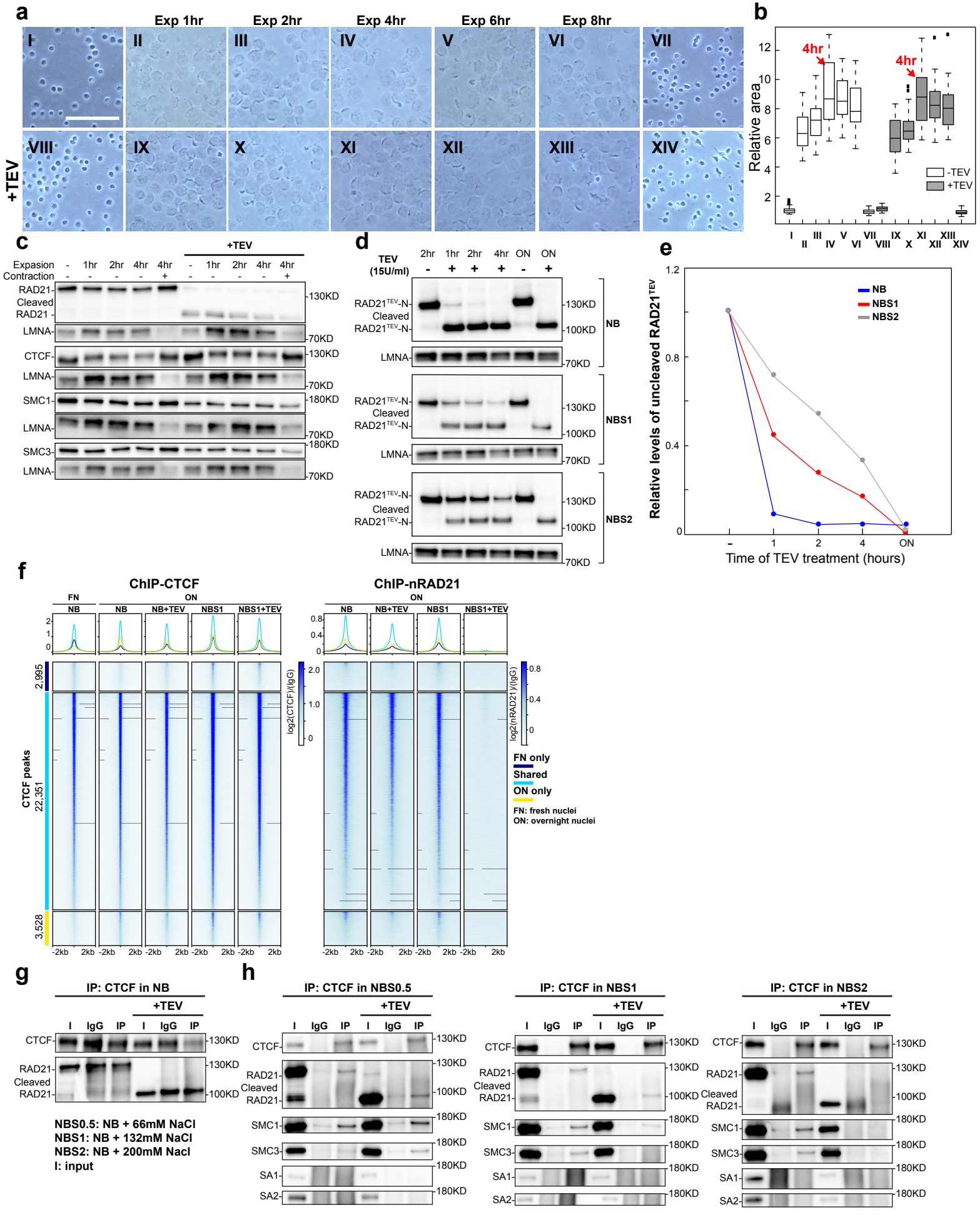

Supplementary Fig. 8

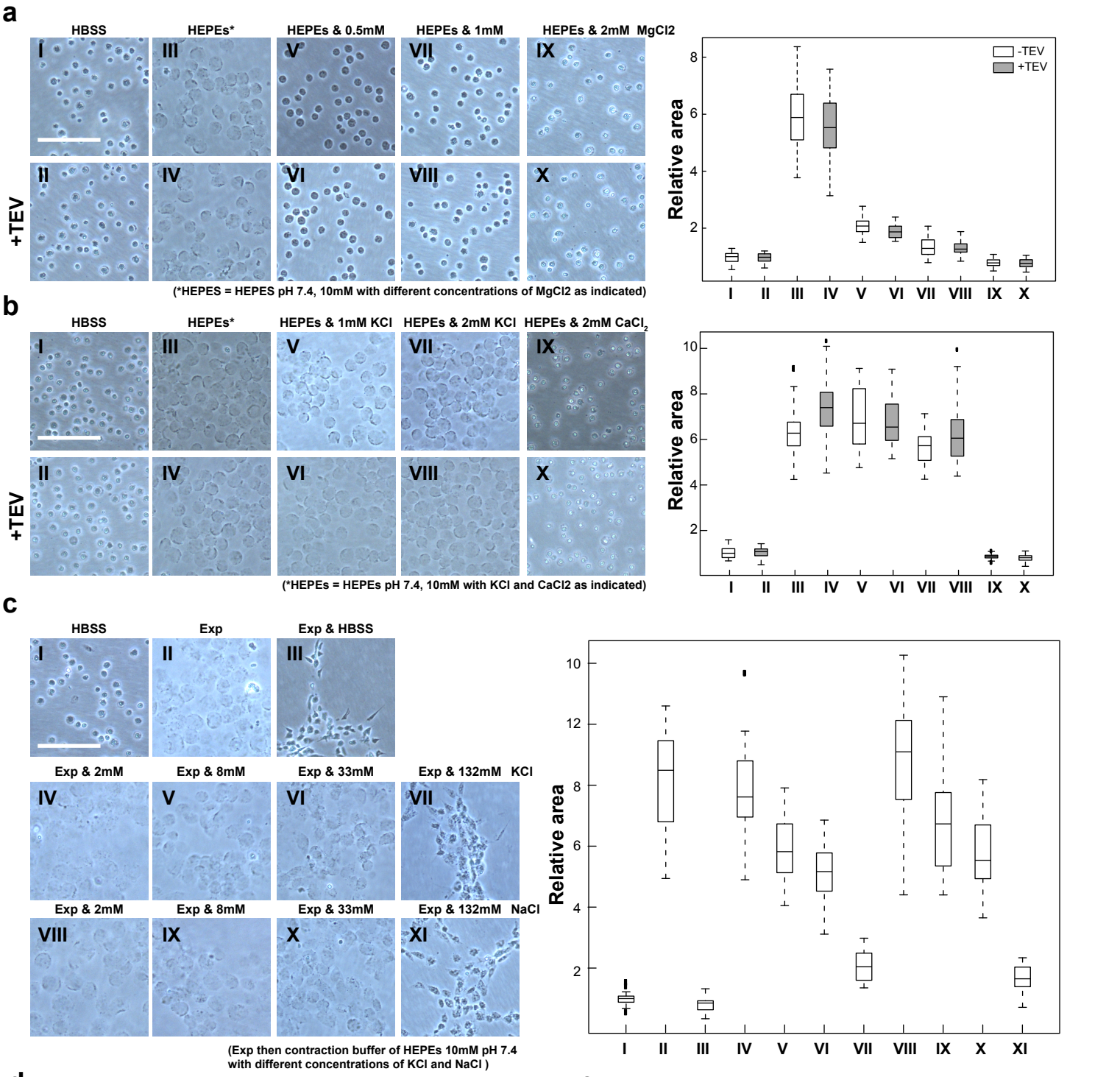

Supplementary Fig. 9

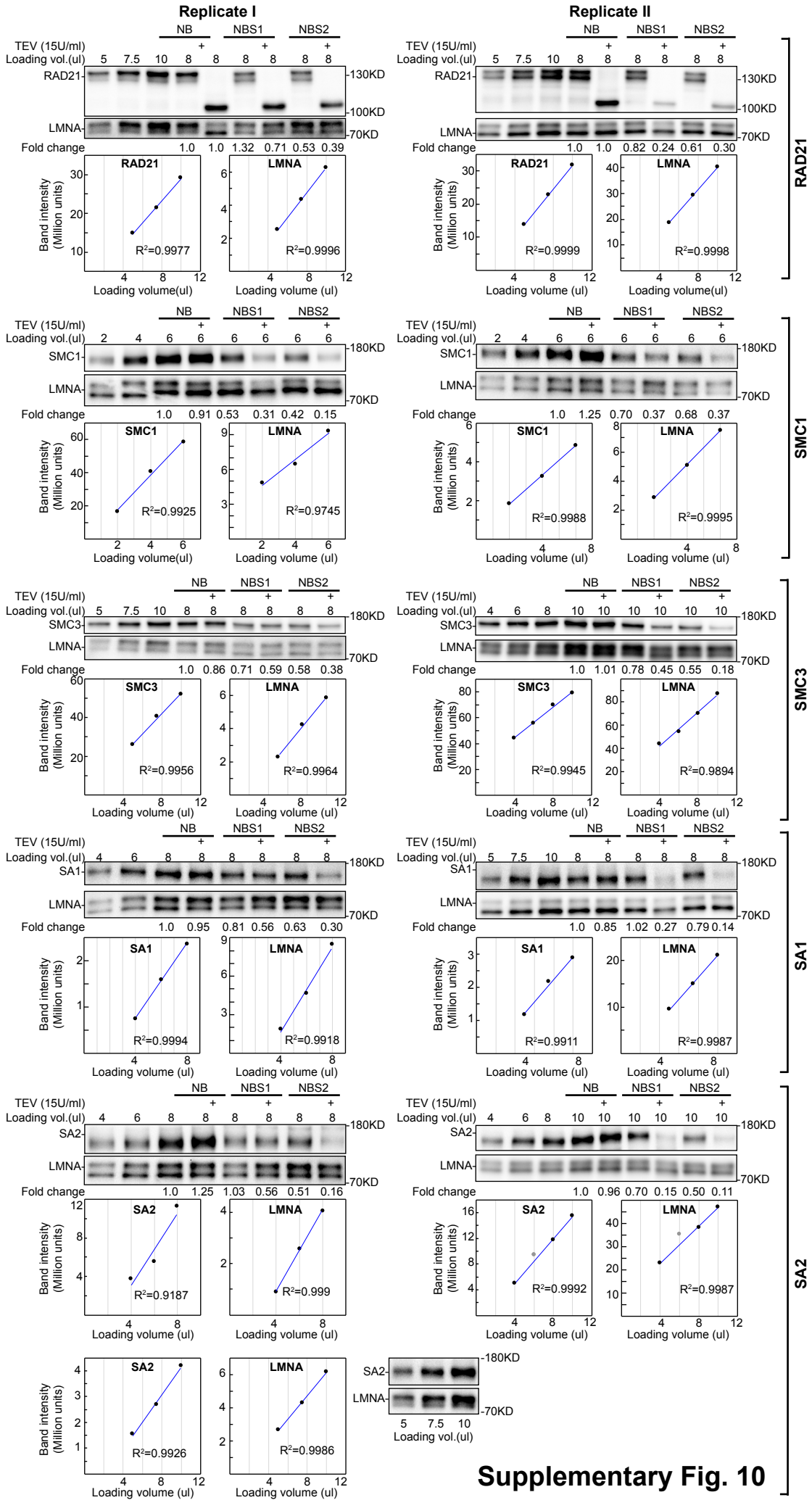

Supplementary Fig. 10

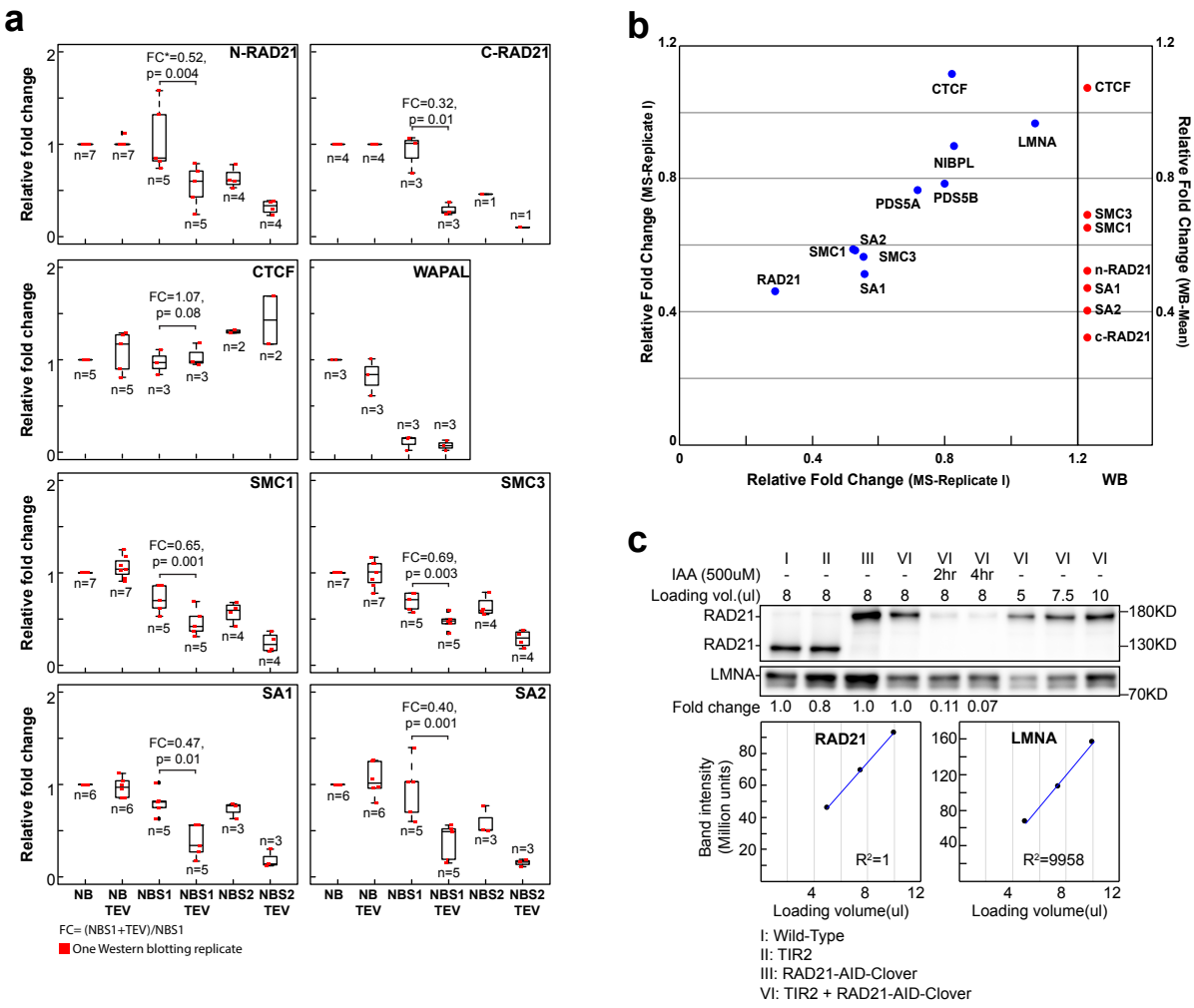

Supplementary Fig. 11

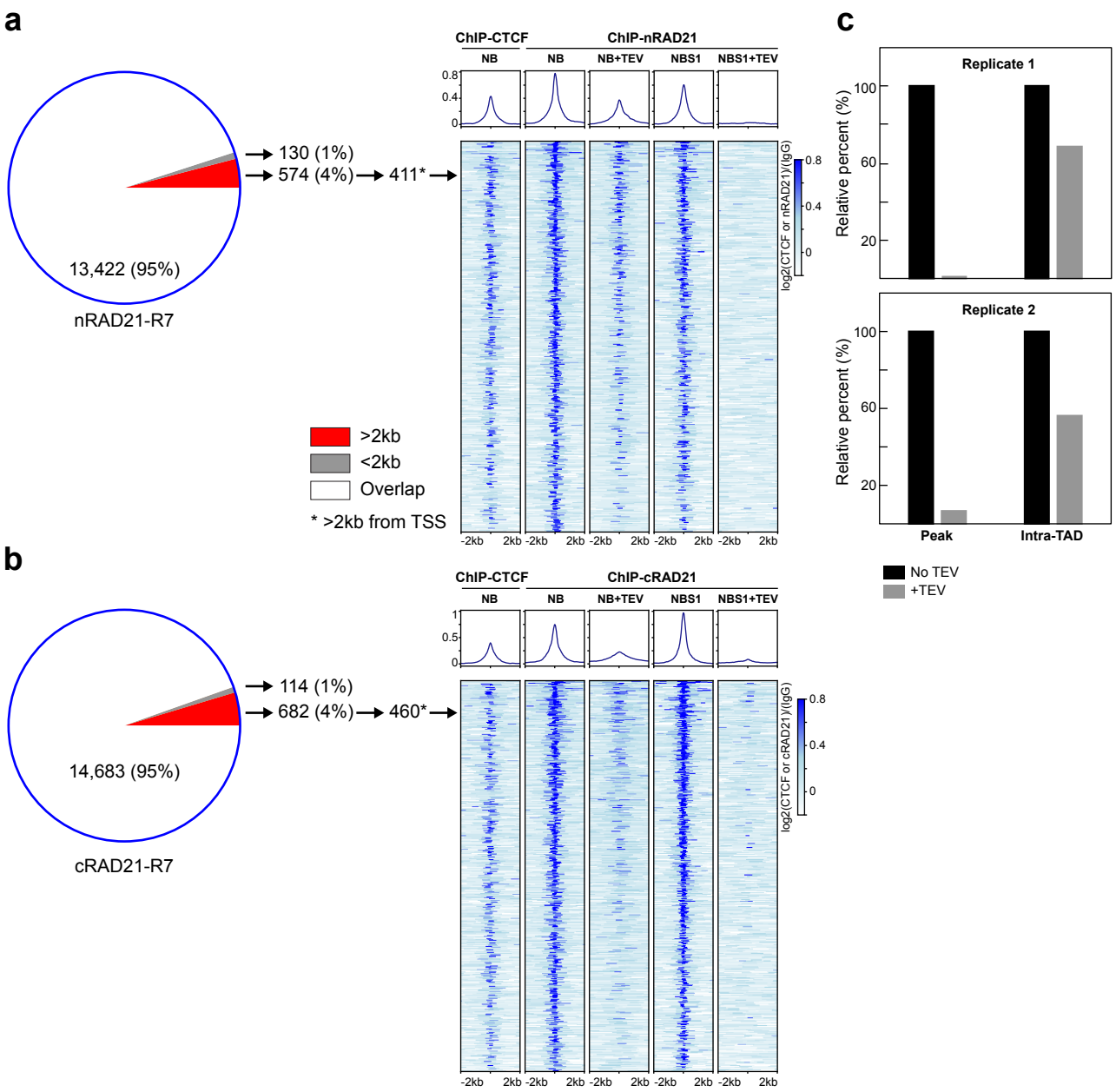

Supplementary Fig. 12

Unprocessed blots for Supplementary Fig. 6a

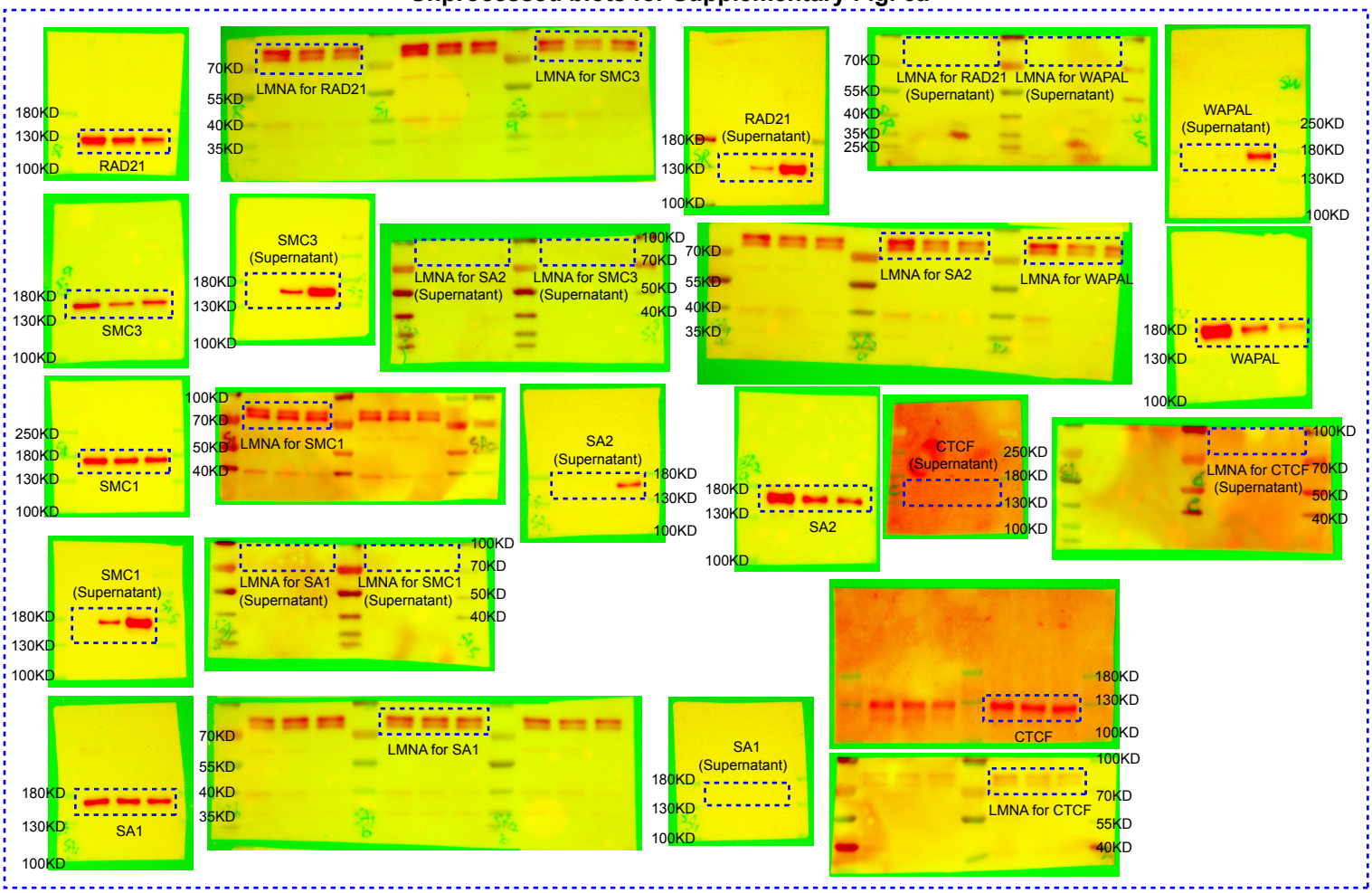

Unprocessed blots for Supplementary Fig. 8c

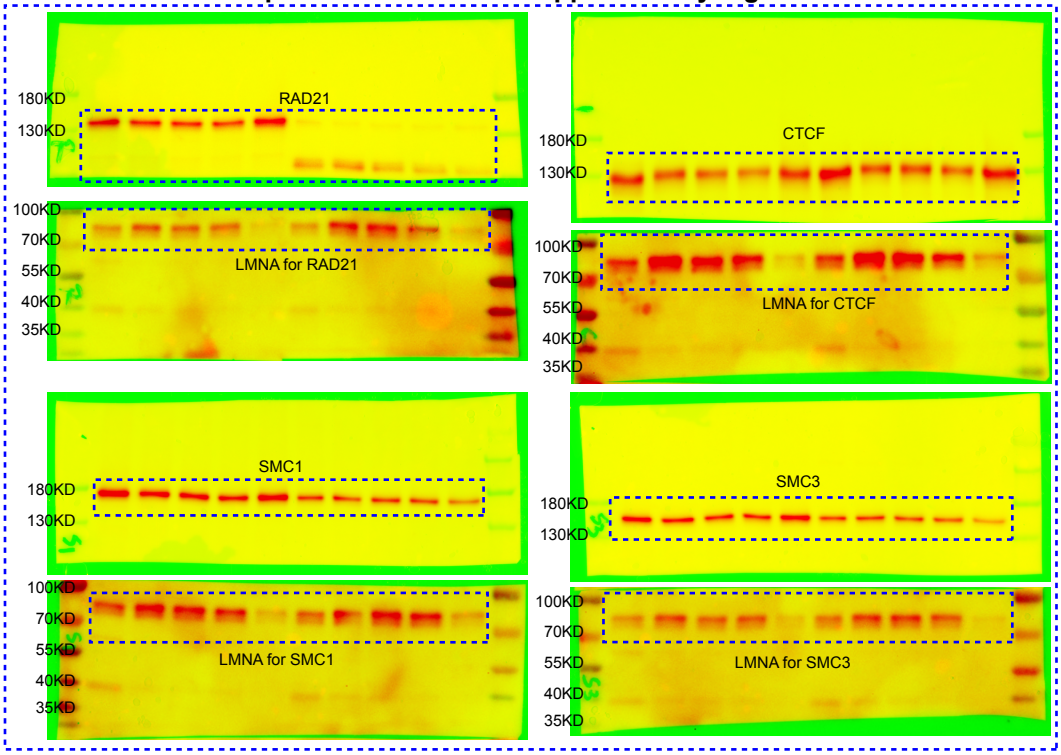

Unprocessed blots for Supplementary Fig. 8d

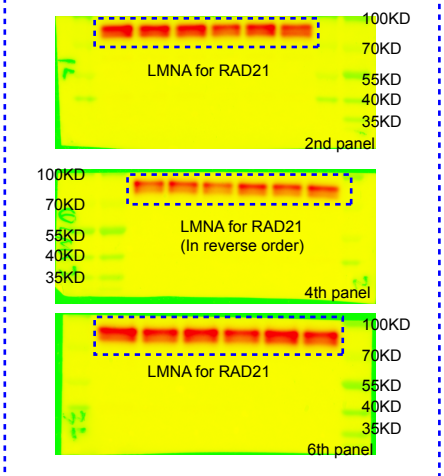

Unprocessed blots for Supplementary Fig. 8g

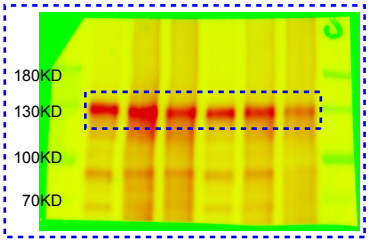

Unprocessed blots for Supplementary Fig. 8h

Left panel

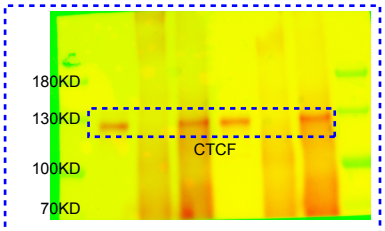

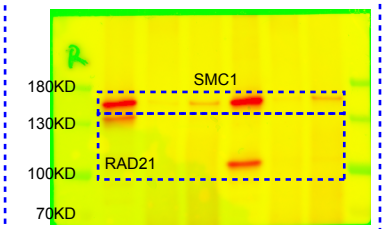

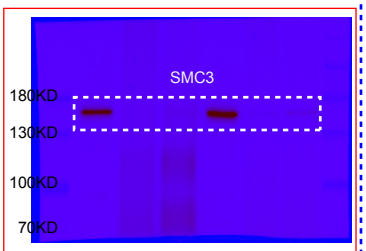

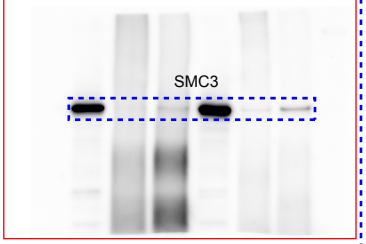

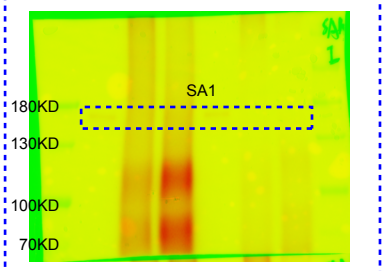

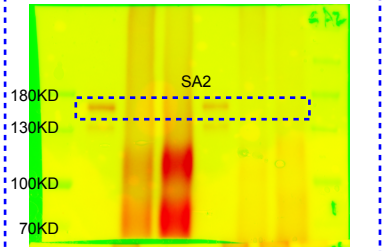

Middle panel

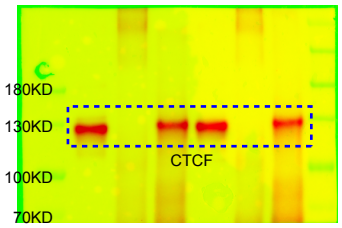

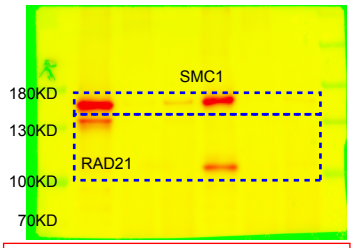

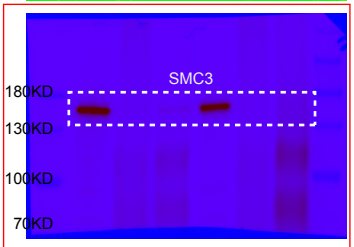

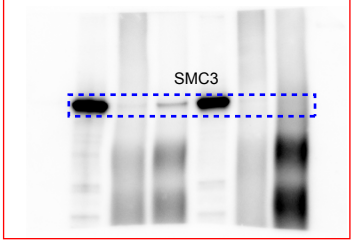

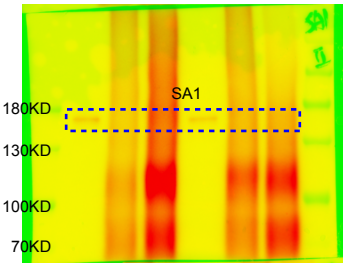

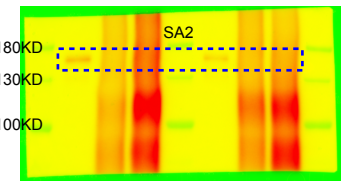

Right panel

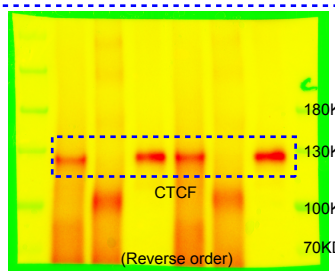

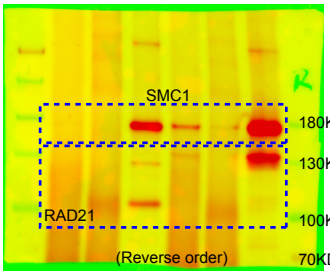

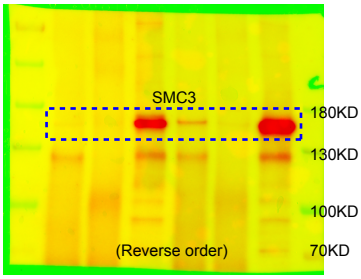

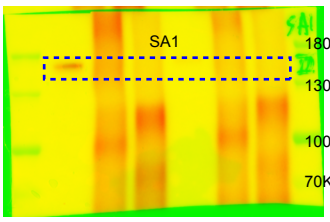

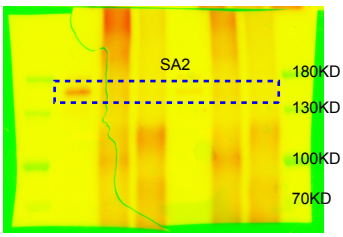

Unprocessed blots for Supplementary Fig. 10a

Left Panels

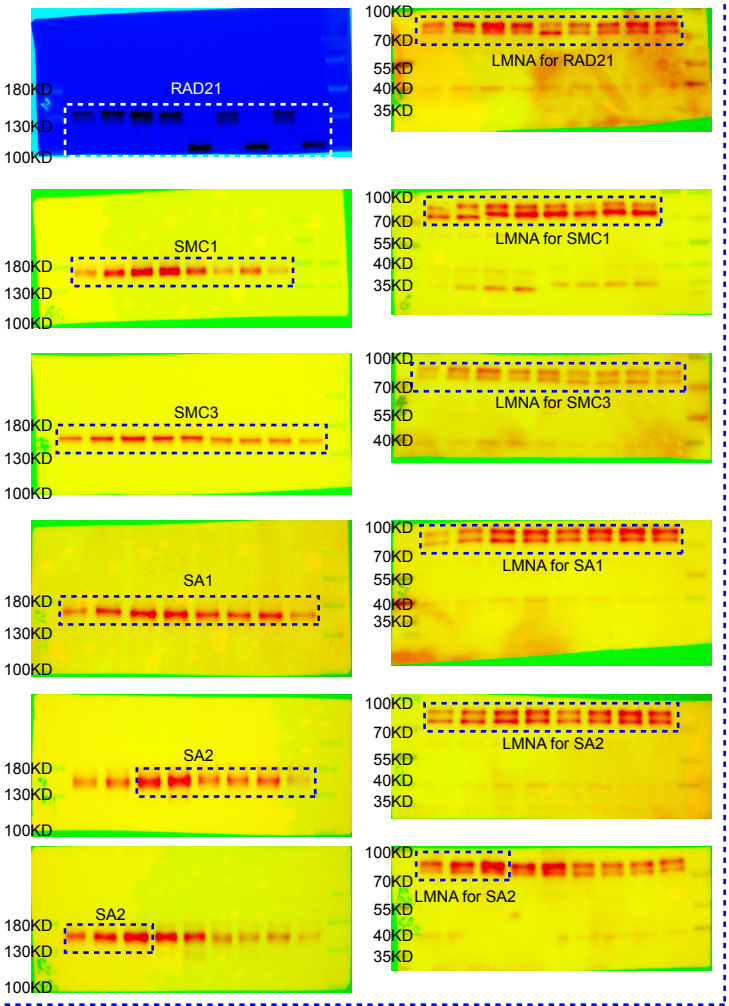

Right Panels

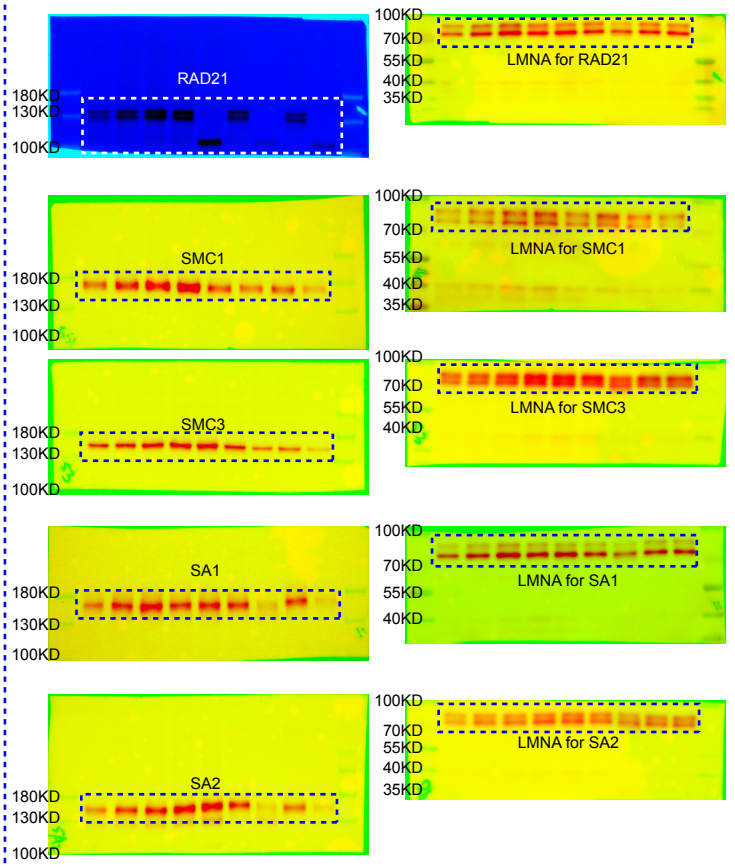

Unprocessed blots for Supplementary Fig. 10d